Journal of Engineering Mathematics **32:** 161–175, 1997.

Local grid refinement in large-eddy simulations

B.J. BOERSMA[1], M.N. KOOPER[2], F.T.M. NIEUWSTADT[1] and P. WESSELING[2]
[1]*Delft University of Technology, Department of Mechanical Engineering, Rotterdamseweg 145, 2628 AL Delft, The Netherlands*
[2]*Delft University of Technology, Department of Applied Mathematics and Informatics, Mekelweg 4, 2628 CD Delft, The Netherlands*

Received 25 October 1996; accepted in revised form 17 February 1997

Abstract. A method for performing nested-grid calculations with a Large-Eddy Simulation (LES) code is described. The grid consists of a coarse mesh and a fine mesh which overlaps the coarse in some region. A standard finite-volume method is used on both meshes. By means of grid communication, the velocity and pressure at both meshes are matched.

To check that large eddies which are already resolved on the coarse grid are not affected by the nesting procedure, a simple two-dimensional mixing layer is simulated. Several simulations of this flow have been carried out with a different number of grid points on the nested grid. It is found that, without much extra computational effort, the grid-nesting improves the turbulent statistics with respect to the results found on the coarse mesh. This improvement occurs first of all in the region where grid refinement is applied, but better results are also found on the coarse mesh outside the grid-refinement region. Furthermore, it is shown that the large-scale structures in this flow are not influenced by the boundary between the coarse and fine grid.

Key words: large-eddy simulations, local grid refinement, turbulence.

1. Introduction

Numerical simulation is becoming an increasingly important tool to study turbulent flows. It is used for instance to investigate fundamental aspects of turbulence, such as coherent structures, but it can also be applied to generate data which can be used to formulate models, *e.g.* closure hypotheses, for a given flow geometry. The most straightforward simulation technique is Direct Numerical Simulation (DNS) in which all turbulent flow scales, *i.e.* from the micro- to the macro-scales, are numerically resolved. However, this approach is limited to low Reynolds numbers. As a result, it is not suited to compute, for instance, engineering or atmospheric flows, which occur at large to very large Reynolds numbers. Therefore, an alternative simulation technique has been developed, namely Large-Eddy Simulation (LES). In this technique the micro-scales of turbulence are removed by means of a filtering procedure and the remaining macro-scales are then numerically solved on a grid of which the size is usually taken proportional to the filter length, see *e.g.* [1] for a review.

The drawback of LES is that the influence of the filtered micro-scales on the resolved macro-scales cannot be neglected. In the filtered equations for the resolved motions this subgrid influence appears as an additional stress term known as the subgrid term. As a consequence, the solution of the LES equations requires a closure hypothesis which gives a description of the subgrid stresses in terms of the known, resolved variables. The subgrid stress is, however, a spatially intermittent and highly fluctuating quantity and its relationship with local flow variables is poorly known. Fortunately, in many circumstances the effect of the subgrid stresses on the large-scale resolved motions is negligible. This is in particular the case when the energy of subgrid motions is small with respect to the total energy of the flow.

In that case we could use a simple subgrid model, because, in view of large-scale dynamics, its only purpose is to dissipate energy at a sufficient rate. Such a simple, but at the same time satisfactory, subgrid closure is the so-called Smagorinsky model [2] which is still widely used.

On the other hand, there are cases where a simple subgrid model fails. The most well-know example is turbulent flow near a wall. The reason is that, as the wall is approached, the turbulence scales, in particular those normal to the wall, become smaller and, consequently, the contribution of the subgrid scales to the total energy becomes larger. Various modifications have been proposed to correct this problem. We may mention here the dynamic model originally proposed by Germano *et al.* [3]. In this model the constant in the Smagorinsky model is adjusted as a function of the spatial coordinates resulting in the subgrid model turning itself off in the neighbourhood of the wall where the flow becomes laminar-like. Another approach is the use of backscatter [4] in which some of the subgrid energy is injected back into the resolved scales by means of a stochastic procedure. However, neither of these modifications is found to be completely satisfactory in all circumstances.

The most straightforward approach to solve the problem mentioned above would be to decrease the filter length of the LES when the wall is approached. In this way we could keep the subgrid energy always small in relation to the resolved energy. A first step toward such a non-uniform filter length would seem to be the use of a non-uniform grid which decreases in size in a direction normal to the wall. However, it appears that in this case the filter length still remains determined by the large grid size of the interior flow. It seems that the non-uniform grid results only in a better representation of the mean profiles as a function of the wall-normal coordinate and not in a better resolution of the turbulence (*e.g.* Nieuwstadt *et al.* [5]).

A real reduction of the filter length can only be obtained when the grid size is reduced in all three coordinate directions. In other words, we need to apply grid refinement. Such a procedure has been proposed by Sullivan *et al.* [6] for a LES of the atmospheric boundary layer. They use a nested grid near the surface which is superposed on and at the same time is collocated with the original coarse grid. Clearly, this is an attractive approach because it allows us to introduce grid refinement at those positions in the flow where the effects of the subgrid model may be critical. In this way, the influence of the subgrid model on the overall results can be reduced.

To perform the computation on both a coarse and a fine grid requires a communication procedure between both grids. An important requirement which such a procedure must satisfy is that it should leave the large eddies which are already resolved on the coarse grid undisturbed. It is the objective of this paper to verify this requirement for two grid-nesting schemes. In the first the communication between both grids is carried out by interpolation, whereas in the second method the procedure proposed by Sullivan *et al.* [6] is used. We consider a particular flow problem for our test, namely the two-dimensional mixing layer which is known to generate large-scale vortex structures. Computation of this mixing layer on both a coarse and a mixed grid, *i.e.* the combination of a fine and a coarse grid, should demonstrate whether the two communication procedures leave the large eddies undisturbed.

The lay-out of this article is as follows. In Section 2, the governing equations for LES will be given and the numerical procedure to solve these equations will be discussed. Next, in Section 3 the details of the grid-refinement procedure will be treated. Finally, in Section 4 the simulation of the mixing layer on which the grid-refinement procedure is tested will be discussed.

2. Large-eddy simulation model

2.1. GOVERNING EQUATIONS

In LES each flow variable ϕ is decomposed in a large-scale component $\overline{\phi}$ and a subgrid scale component ϕ' as $\phi = \overline{\phi} + \phi'$ where the large-scale component is obtained by the application of a moving-filter operation. The resulting equations for the spatially filtered velocity, $\overline{u_i}$, and pressure, $\overline{p}$, then become:

$$\overline{u}_{i,i} = 0, \tag{1}$$

$$\frac{\partial \overline{u}_i}{\partial t} + (\overline{u}_i \overline{u}_j)_{,j} = -\frac{1}{\rho}\overline{p}_{,i} + \nu \overline{u}_{i,jj} + \tau_{ij,j}, \tag{2}$$

where ρ is the density of the fluid. In this equation a new stress term appears, the so-called subgrid stress τ_{ij}. It is defined as

$$\tau_{ij} = -(\overline{u_i u_j} - \overline{u}_i \overline{u}_j). \tag{3}$$

We parametrize this subgrid stress here following the Smagorinsky model:

$$\tau_{ij} = 2\nu_t \overline{S}_{ij} \quad \text{with} \quad \nu_t = (c_S \Delta)^2 \sqrt{2\overline{S}_{ij}^2}, \tag{4}$$

where $\overline{S}_{ij}$ is the deformation-rate tensor of the resolved velocity field

$$\overline{S}_{ij} = \frac{1}{2}\left(\frac{\partial \overline{u_i}}{\partial x_j} + \frac{\partial \overline{u_j}}{\partial x_i}\right). \tag{5}$$

In the equation for ν_t, the Δ is a representative grid spacing which is defined here as $\Delta = (\Delta x_1 \Delta x_2 \Delta x_3)^{1/3}$, where the Δx_1, Δx_2 and Δx_3 are the grid spacings in the three coordinate directions. The constant c_S is known as the Smagorinsky constant and it can be interpreted as being proportional to the ratio of the filter length to the grid spacing. In general a value $\sim 0{\cdot}1 \ldots 0{\cdot}2$ is taken for c_S which implies a filter length of approximately twice the grid spacing.

2.2. COMPUTATIONAL METHOD

The equations given in the previous subsection are solved by the following numerical techniques. The Equations (1)–(2) are discretized with a second-order finite-volume method on a staggered grid. A second-order Adams–Bashforth [7] method is used for the time integration. Keeping the Courant number fixed, we adjust the time step dynamically. Mass conservation is preserved through a pressure-correction method [8]. This leads to the following system of equations to be solved consecutively:

$$u_i^* = u_i^n + \triangle t\ (\tfrac{3}{2}A(u_i^n) - \tfrac{1}{2}A(u_i^{n-1})), \tag{6}$$

$$-Du_i^* = -\triangle t\ DGp^{n+1}, \tag{7}$$

$$u_i^{n+1} = u_i^* - \triangle t\ Gp^{n+1}. \tag{8}$$

Here, u_i^n is the velocity at time $n\triangle t$ and p^n the pressure. The operator $A(u_i^n)$ represents the discretized viscous and convective terms; D is the discrete divergence operator and G the discrete gradient operator. The Poisson equation (7) needs to be solved at every time step by an iterative or direct solver. Here, we have used a direct solver based on Fast-Fourier-Transform techniques (e.g. [9,10]).

3. **Grid-nesting algorithm**

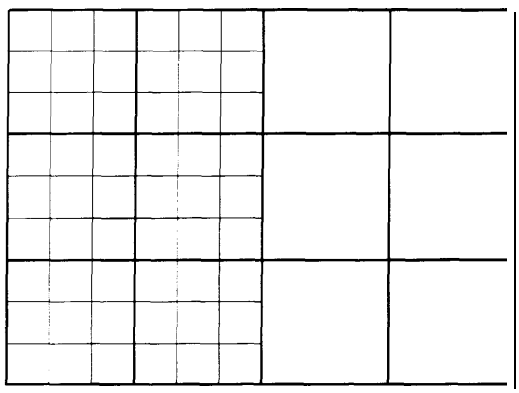

Figure 1. A fine grid nested within a coarse grid

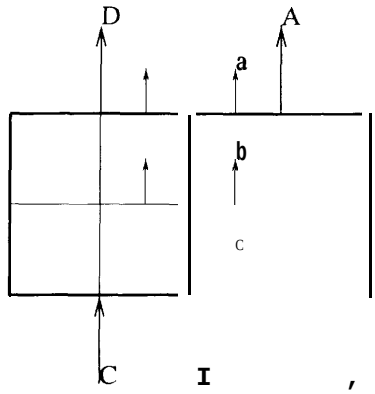

Figure 2. Interpolation of the tangential velocity components from the coarse grid to the fine grid.

The purpose of local grid refinement is to obtain a better resolution of turbulence in areas which can be considered as critical in terms of the total flow problem. The starting point is a numerical simulation of the whole flow field on a coarse uniform grid. In some parts of the flow domain, which are considered to be critical, the coarse grid is locally overlaid with a fine grid. The fine grid is also taken to be uniform. This grid structure is shown in Figure 1. The coarse grid size is a multiple of the fine grid size, so that each coarse cell is a union of fine cells. On both grids the standard staggered velocity representation as discussed above is used.

3.1. COMMUNICATIONFROMTHECOARSETOTHEFINEGRID

An important problem is to know how the interaction between the two grids should be formulated and various methods can be devised for this. Here, we consider the interaction imposed through conditions on the boundaries between the fine and the coarse grid. These boundaries either coincide with a physical boundary or they are embedded in the interior of the coarse grid. In the former case, the standard boundary conditions, used on a surface, are applied both on the fine and coarse grid. For the latter case, i.e. the interior boundary, Dirichlet conditions are applied: i.e. on the boundary of the fine grid velocity components are prescribed. These boundary conditions need to be adapted every time step. They follow from interpolation of the velocity computed on the coarse grid.

Let us specify this interpolation procedure in somewhat more detail. For simplicity we shall consider interpolation in two-dimensions and for a grid refinement factor of two (generalisation to three dimensions and to other grid refinement factors is straightforward). Boundary conditions for the velocity components tangential to thc interface are implemented by intro-

duction of virtual points outside the area of the fine grid, *cf.* Figure 2. Next, a multi-linear interpolation[1] is computed according to

$$v_a = (3v_A + v_D)/4, \qquad v_c = (3v_B + v_C)/4, \qquad v_b = (v_a + v_c)/2, \tag{9}$$

with v_a, v_b and v_c as the velocities on the fine grid and v_A,v_B, v_C and v_D as those on the coarse grid.

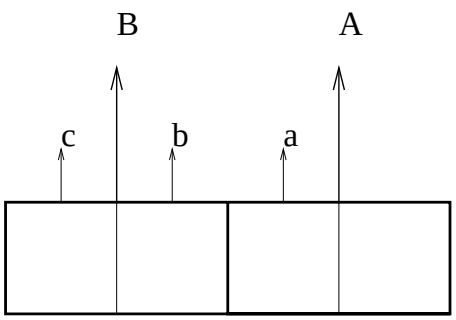

Figure 3. Interpolation of the normal velocity components from the coarse grid to the fine grid.

Following Thompson and Ferziger [11], we use for the normal velocity components a slightly different procedure to ensure mass conservation. First, preliminary values, denoted by primes, are computed by multilinear interpolation (Figure 3)

$$u'_a = (3u_A + u_B)/4, \qquad u'_b = (u_A + 3u_B)/4, \tag{10}$$

with the same notation as used above. Next, a correction is applied to ensure that the sum of the mass flux through the fine-grid cell faces of which the union is a coarse grid-cell face, equals the original mass flux through this coarse-grid cell face. For the situation depicted in Figure 3, this implies $(u_b + u_c)/2 = u_B$. We achieve this by defining

$$u_b = \frac{2\,u_B}{u'_b + u'_c} u'_b, \qquad u_c = \frac{2\,u_B}{u'_b + u'_c} u'_c.$$

3.2. COMMUNICATION FROM THE FINE TO THE COARSE GRID

Not only do we have to take into account the influence from the coarse grid on the fine grid by means of the boundary conditions, but we need also an update of the coarse-grid velocity components by the results obtained on the fine grid. Two possible coupling methods between the grids which we will consider are:

Method 1

In this method we apply interpolation of the results of the fine grid to the coarse grid. This interpolation may take place at arbitrary time steps to be determined by the user. In our

[1] It would appear that a second-order interpolation scheme is required in order not to destroy the accuracy of the numerical solution on the fine grid. However, the subgrid-stress modeling introduces a first-order, local error and, therefore, we concluded that a first-order interpolation would be sufficient. Indeed, we typically found no visible influence of this local error on the results in our simulations (See results in Section 4).

simulations we applied this interpolation at every time step, but we may get by with less interaction. Interpolation could be applied after the predictor step ($u_f^* \rightarrow u_c^*$), or after the correction step ($u_f^{n+1} \rightarrow u_c^{n+1}$). Since the latter, which is also known as a so-called *post-insertion* method, may violate the conservation of mass on the coarse grid, we prefer to interpolate after the predictor step.

To illustrate the interpolation algorithm, a description of all steps is given in the Appendix A.

Method 2

In the paper of Sullivan *et al.* [6] another method of so-called two-way coupling between the coarse and the fine grids is proposed. In their case communication from the fine to the coarse grid is taken care of by modification of the subgrid terms in the coarse-grid equations. These terms, which appear both in the coarse-grid momentum equations and in the right-hand side of the Poisson equation for the pressure, are now formulated in terms of the subgrid model on the fine grid together with an explicit contribution of the scales in between the large and small grid. It turns out that this formulation is consistent with the filtering procedure introduced by Germano *et al.* [3] in their dynamic model.

To illustrate this algorithm, a description of all steps is given in Appendix B.

4. The mixing layer

4.1. PROBLEM DESCRIPTION

The LES model including the grid-refinement technique described in the previous section will be tested for the case of a horizontally homogeneous, two-dimensional mixing layer which develops as a function of time. This flow is also known as a temporal mixing layer. One might perhaps object that a two-dimensional flow will not lead to the turbulence that we usually aim to simulate with LES. However, we have selected this case because of the fact that, in a two-dimensional temporal mixing layer, the flow as a function of time organizes itself in large-scale vortex structures. Our purpose is to check with this flow whether our grid-refinement procedure leaves these large-scale vortex structures and their development, which is already well resolved on the coarse grid, undisturbed. In our opinion, this should be checked first before we can apply the grid-refinement technique with confidence to three-dimensional turbulence in order to improve the resolution of small-scale turbulence[2].

For the formulation of the temporal mixing-layer problem, we follow Lesieur *et al.* [12] who have performed DNS of such a mixing layer at the high resolution of 256×256 grid points, using a streamfunction-vorticity formulation with a hyperviscosity subgrid model. Here, we consider a two-dimensional mixing layer in the x, y plane at $y = 0{\cdot}5$ in a box $0 < x, y < 1$. At the upper and lower boundaries, *i.e.* at $y = 0$ and $y = 1$ we apply free-slip

[2] It should be stressed that in this article we primarily concentrate on the behaviour of the large resolved scales under grid refinement and for this we have selected the two-dimensional mixing layer. The difference between the two grid-communication methods discussed in Section 3.2 will appear in particular when the subgrid scales play a more important role in the flow dynamics such as in the case of three-dimensional turbulence. Therefore, we should be careful in interpreting the results obtained with these two grid-communication methods here in terms of their performance in the three-dimensional case and for the latter we refer to [6].

boundary conditions. In the x-direction we use periodic boundary conditions. At the initial time, *i.e.* $t = 0$, the velocity field is given by:

$$U(y) = U_\infty \tanh\left(\frac{2y-1}{\delta}\right), \tag{11}$$

where δ is chosen as:

$$\delta = \frac{1}{28} \approx \frac{0{\cdot}8892}{16\pi}. \tag{12}$$

In this case, the wave number of the fastest growing spatial mode α_a is equal to 16π. On the initial velocity field (11) we superpose a perturbation with components u and v, defined by means of a stream function according to

$$u = \frac{\partial \psi}{\partial y}, \qquad v = -\frac{\partial \psi}{\partial x}. \tag{13}$$

and, as a result, the perturbation is divergence-free. The perturbation stream function is given by

$$\psi = 0{\cdot}1 U_\infty \exp\left[-\left(\frac{y-0{\cdot}5}{\delta}\right)^2\right] \cos(\alpha x), \tag{14}$$

in which the wave number is $2\pi/\lambda$ with a wave length λ. We have taken for the actual perturbation the sum of two waves with wave lengths 1/4 and 1/10 in terms of the domain length, respectively. The Reynolds number of this flow is defined as $\mathrm{Re} = U\delta/\nu$ where ν is the kinematic viscosity of the fluid. In all simulations Re was taken equal to 250. In the following, the results shall be presented in terms of non-dimensionalized time, *i.e.* the time scaled with δ/U_∞.

4.2. SIMULATIONS

Six different simulations have been carried out for the flow geometry of the temporal mixing layer discussed above. In each simulation we have changed the number of grid points and in a number of cases we have used our grid-refinement procedure. In the cases 1 to 4, we have used coupling method 1 and cases 5 and 6 have been calculated with coupling method 2. The computational details of all cases are collected in Table 1.

Table 1. The different grids used in the simulations

	a	b	c	d	e	f
N_{coarse}	240 × 240	80 × 80	80 × 80	80 × 80	80 × 80	80 × 80
y (fine)	–	–	$\frac{3}{8} < y < \frac{5}{8}$	$\frac{3}{8} < y < \frac{5}{8}$	$\frac{3}{8} < y < \frac{5}{8}$	$\frac{3}{8} < y < \frac{5}{8}$
N_{fine}	–	–	160 × 40	240 × 60	160 × 40	240 × 60
C_s	0·1	0·1	0·1	0·1	0·1	0·1
Cpl. meth.	–	–	1	1	2	2

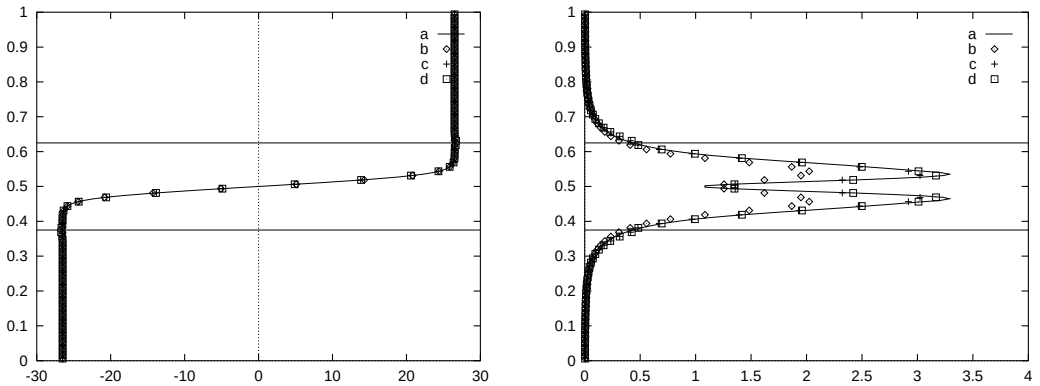

Figure 4. The mean velocity profiles after 20 timescales (left). The profiles of the root mean square of the streamwise velocity fluctuations after 20 timescales (right).

The first computation, denoted as case a, uses a grid consisting of 240 $\times$ 240 grid points with no grid refinement. This high-resolution computation is taken as a reference with which the other computational data are to be compared. In the second case, denoted as case b, a coarser grid of 80 $\times$ 80 has been used and again no grid refinement has been applied. This case allows us to estimate the improvement of grid refinement on the computational results. The next two computations, cases c and d, are both computed on the grid of 80 $\times$ 80 grid points in combination with the grid-refinement procedure according to method 1 of Section 3.2. In computation c, the grid refinement was applied in the sub domain $0 < x < 1$ and $0{\cdot}375 < y < 0{\cdot}625$, *i.e.* around the velocity discontinuity. The refinement factor is 2 in both directions. In computation d the grid refinement has been applied to the same sub domain, but now with a refinement factor of 3 in both directions. The last two computations e and f use the same number of grid points as c and d, but the difference lies in the grid-communication method which is now method 2.

For most applications it is sufficient to consider statistical quantities, like mean flow profiles, root mean square profiles and spectra. Therefore, we will restrict ourselves to a comparison of these variables on the coarse and refined grid with the results obtained for high-resolution case a.

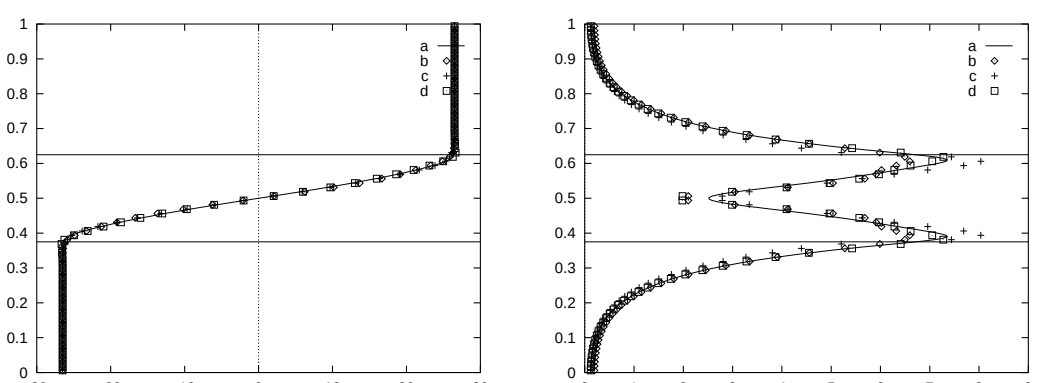

Figure 5. The mean velocity profiles after 40 timescales (left). The profiles of the root mean square of the streamwise velocity fluctuations after 40 timescales (right).

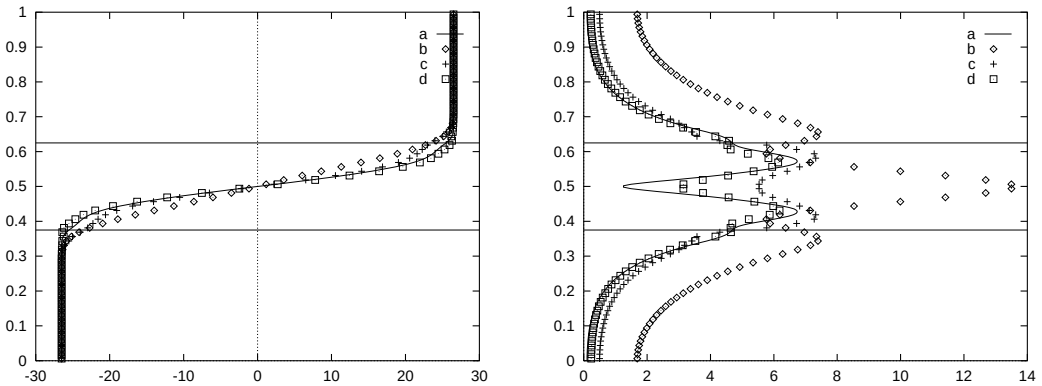

Figure 6. The mean velocity profile after 60 timescales (left). The root mean square profiles of the streamwise velocity after 60 timescales (right).

In Figure 4 (left) we have plotted the mean velocity profiles obtained from the four simulations a–d after 20 timescales. In Figure 4 (right) similar results are shown, but now for the root mean square (rms) of the velocity fluctuations after 20 timescales. All four simulations give almost identical profiles for the mean velocity but some differences show up for the rms values. The fact that the numerical resolution of simulation b is lower than for case a is clearly reflected in the smaller magnitude of the rms for case b. However, the simulations c and d, which use grid refinement, give rms values comparable with the results of simulation a on the fine grid.

In Figures 5 and 6 (left and right) we have plotted the mean and rms profiles for the cases a–d after 40 and 60 timescales, respectively. All four simulations give again identical mean flow profiles after 40 timescales, and there is reasonable agreement for the rms profiles. After 60 timescales some differences become apparent in the mean profiles. However, it is clear that in comparison to the high resolution case a, the nested-grid simulations, *i.e.* simulations c and d show better agreement than the non-nested coarse simulation b. Figure 6 (right), which illustrates the rms-profiles after 60 timescales, shows very clearly that the nested-grid simulations c and d are superior to the coarse-grid simulation b. The interesting fact, which should be noted here, is that the results improve not only in the region where the grid refinement has been applied, but also in the regions where the grid has remained coarse. Furthermore, it is also clear that simulation d gives better results than simulation c, *i.e.* an increasing value of the grid-refinement factor or a increasing number of gridpoints on the fine patch, improves the results. Again, this improvement is found both within and outside the region of grid refinement.

The results for the cases c–d above have been calculated by coupling method 1 of Section 3.2, *i.e.* the method with interpolation of the fine grid results to the coarse grid. In Section 3.2 we have also presented another coupling method, indicated as method 2. In this second method, the fine grid solution is used to calculate the subgrid stresses on the coarse grid in the nested region. The use of a subgrid model on the coarse grid in the overlap region is thus avoided. The performance of method 2 is considered in computations e and f which have the same grid resolution as cases c and d, respectively.

In Figure 7 we show the root-mean-square values of the streamwise velocity at $t = 40$ and $t = 60$ for cases e and f. For comparison, we have again plotted in this figure the fine-grid simulation (a). The agreement between the nested-grid simulations and the fine-grid

simulation by means of coupling method 2 is for case f comparable with the results obtained with coupling method 1 (see Figures 5 and 6). For case e the results with method 2 seem to be somewhat poorer, which is due to the computation in method 2 of the scales in between the large and small grid. However, before making any conclusion regarding the performance of the two coupling methods, we should remind the remarks made in footnote 2.

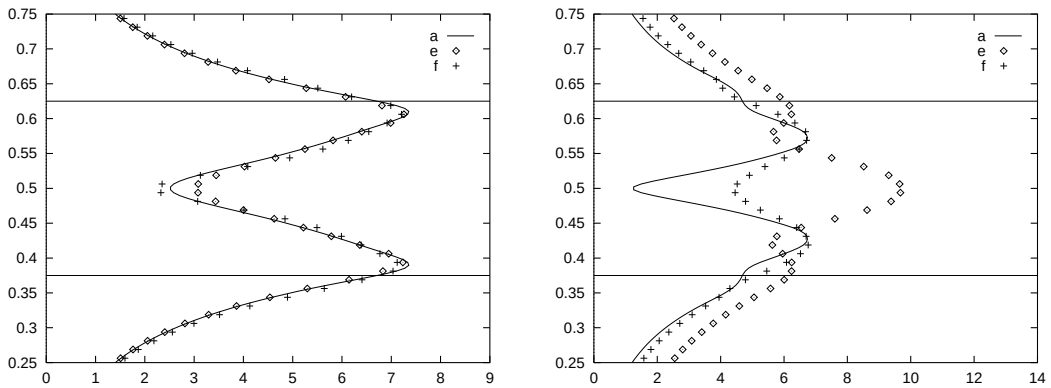

Figure 7. The root mean square profiles of the streamwise velocity after 40 and 60 timescales. Calculated with coupling method 2

4.3. VORTICITY

Another interesting quantity for analysis is the vorticity. In two dimensions only one component of the vorticity vector differs from zero. In our case this is ω_z defined as

$$\omega_z = \frac{\partial(U+u)}{\partial y} - \frac{\partial v}{\partial x}. \tag{15}$$

In each of the Figures 8, 9 and 10 we show contour plots of the vorticity for the simulations a–d after 20, 40 and 60 timescales, respectively. The data for the cases c and d at 20 timescales show qualitatively the same behaviour as simulation a given in the same figure. On the other hand, the vortex pattern for the coarse-grid is clearly different. In fact, the pairing of the vortices has already started in this coarse-grid case, caused by a numerical resolution that is too low which leads to numerical damping that is too high. After 40 timescales the agreement between simulations a, c and d is still good, while simulation b shows a totally different behaviour. After 60 timescales only an acceptable agreement between simulations a and d remains.

4.4. SPECTRA

A more detailed comparison between the results obtained on the different grids can be made with help of the energy spectrum. Since the mixing layer is periodic in the x-direction, we can calculate one-dimensional spectra along this axis. The one-dimensional energy spectrum averaged over the y-direction then reads, (*e.g.* Lesieur *et al.* [12] Equation 2.5):

$$E(k) = \int_0^1 |\hat{u}(k,y)|^2 \, \mathrm{d}y, \tag{16}$$

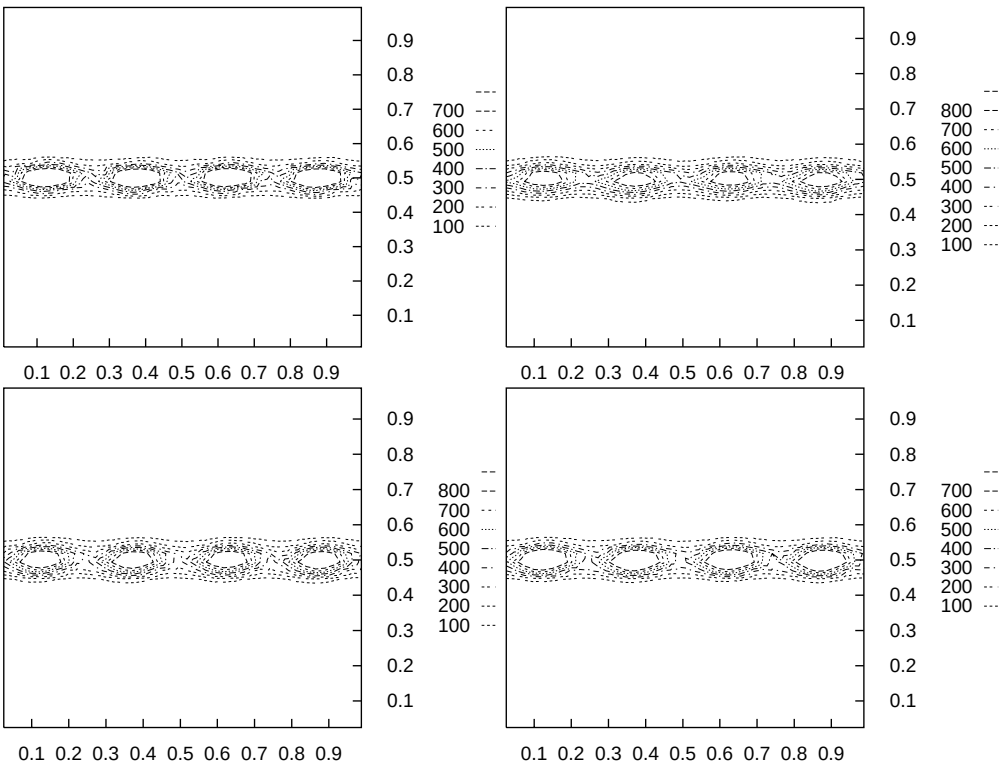

Figure 8. Contour lines of the vorticity after 20 timescales

where

$$\hat{u}(k,y) = \frac{1}{N}\sum_{k=0}^{N} u(x,y)\,\mathrm{e}^{-ikx}, \tag{17}$$

is the Fourier Transformation of the velocity in the x-direction.

In Figure 11 we show these energy spectra for the cases a–d after 40 timescales. The spectrum for the the fine grid simulation a given by the solid line, should be again taken as a reference. The spectrum for the coarse grid, case b, clearly fails for the smallest scales, *i.e.* the highest wave numbers. The two cases, with grid-refinement, show much better results in comparison with a. Against our expectation the agreement is best for case c which uses a lower grid-refinement factor than case d. The interpolations from the fine to the coarse patch probably introduce some noise which increases with the grid-refinement factor. In this figure we have also plotted a line with a slope of -4, which is the behaviour of the spectrum observed by Lesieur *et al.* [12]. We see that all simulations agree more or less with such k^{-4} behaviour.

5. Concluding remarks

It has been argued that Large-Eddy Simulation becomes less reliable near physical boundaries like walls, where the length scales of the large eddies are reduced and a finer grid is needed to resolve these eddies. In this paper we have proposed a method which can be used to refine a grid locally in all *three* directions, by means of a so-called grid-nesting method. In this

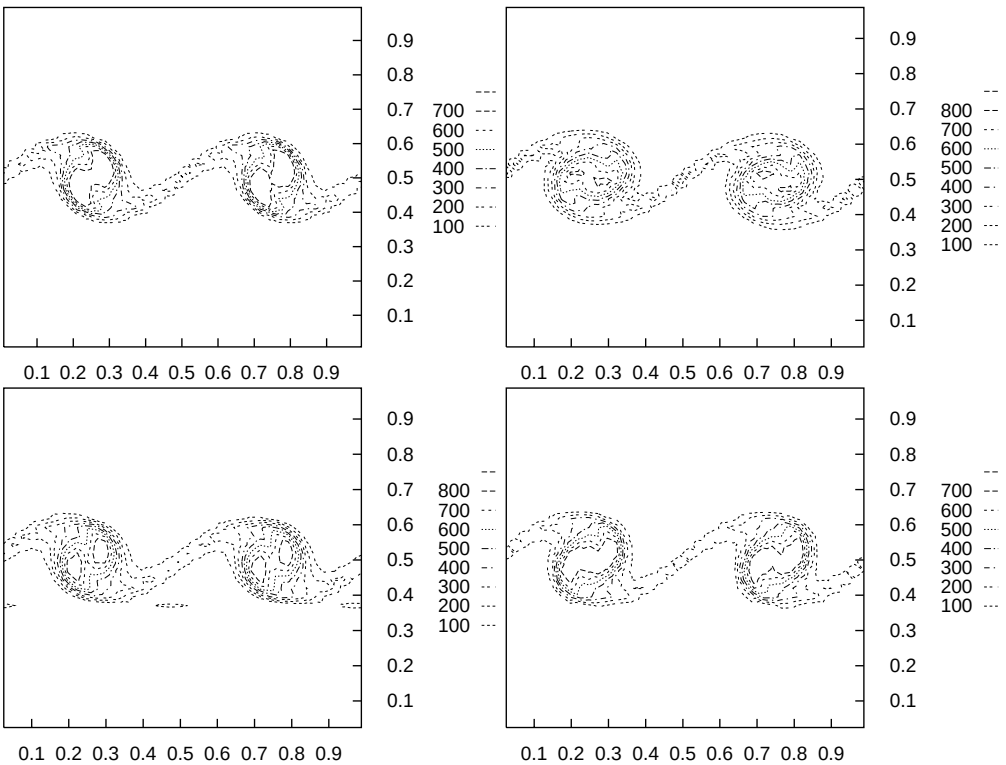

Figure 9. Contour lines of the vorticity after 40 timescales

method, a coarse grid and one or more fine grids are used which overlap the coarse grid in some part of the flow domain.

In the present study simulations for a two-dimensional temporal mixing layer have been carried out with varying resolutions on the fine-mesh. The results from this grid-refinement procedure have been compared with the results of a high-resolution simulation carried out on the same flow domain. This particular flow has been selected because it allows us to study whether the grid-refinement procedure influences large-scale structures in the flow.

From the results we can conclude that with respect to statistics such as the mean velocity and the rms values, the nested grid simulations are clearly superior to the results obtained with a simulation on a coarse grid in the whole flow domain. Contour-line plots of the vorticity show no visible influence of the boundary between the coarse and fine grids. Also, the one-dimensional spectra confirm that the results of the refined-grid computations perform better in comparison with the coarse-grid computations.

Therefore, we venture to conclude that the grid-nesting procedure seems to meet its objective, namely a local increase of resolution. However, we again stress that our comparison here has been carried out for a two-dimensional flow. It has still to be checked whether our conclusion also applies to the three-dimensional case. In this case we expect that the communication from the fine to the coarse grid will play a more important role than in the present case. This will be the subject of further study.

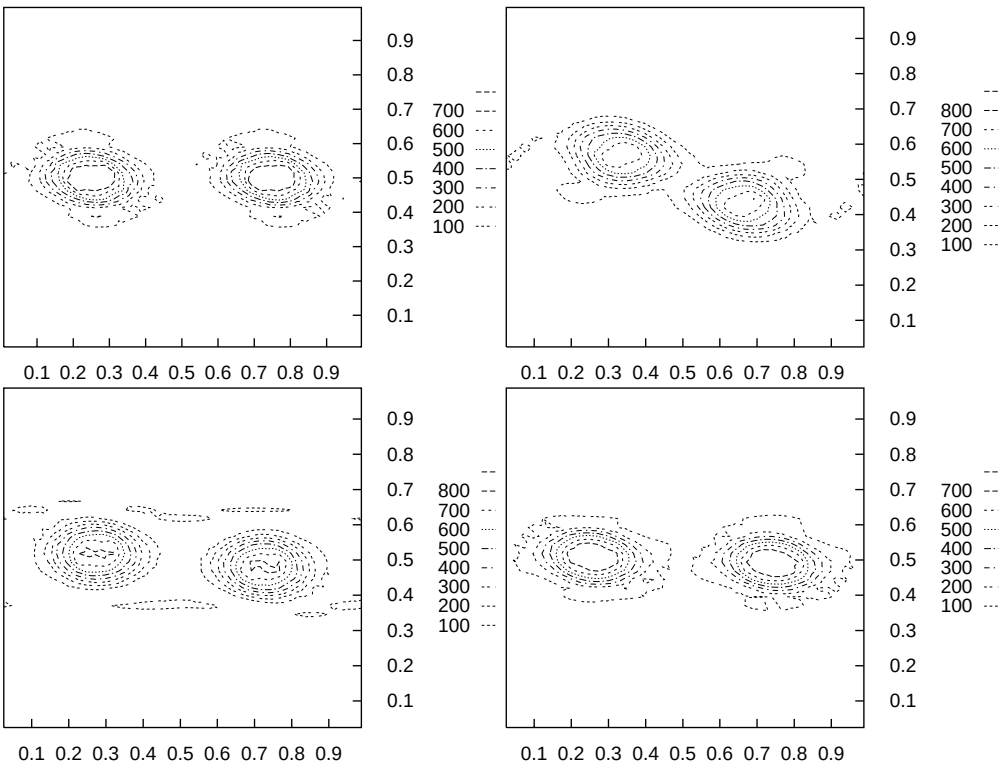

Figure 10. Contour lines of the vorticity after 60 timescales

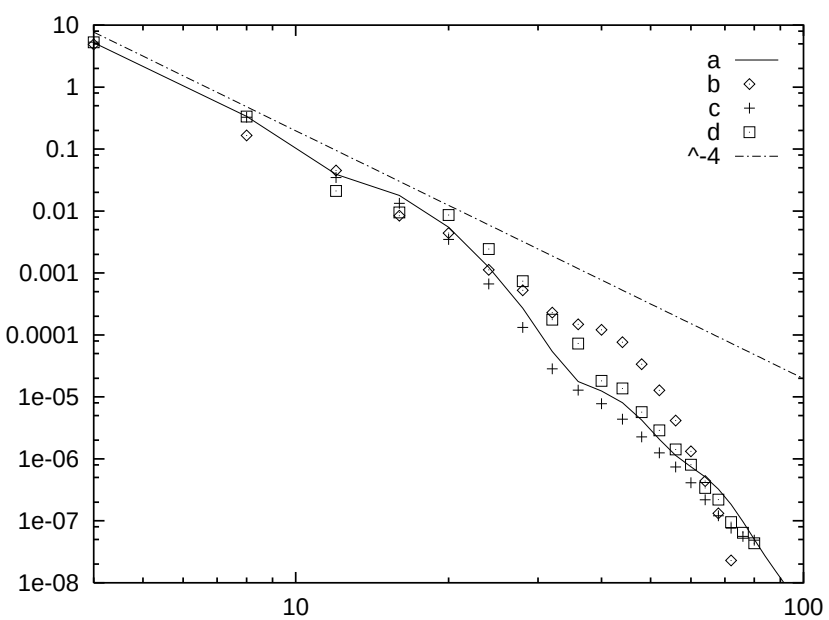

Figure 11. The one-dimensional energy spectra as defined by Equation (17)

Acknowledgements

The first author wants to thank the Dutch Foundation of Technology (STW) for their financial support under grant DTN22.2646. The second author was supported by an EZ-grant from the J.M. Burgers Centre.

Appendix A: Grid-nesting algorithm (1)

1. Initialize u_c^0 and u_f^0.
2. For $n = 1$, nstep do
   (a) Calculate the turbulent viscosity ν_t on the coarse grid.
   (b) Apply boundary conditions on the coarse grid for the velocities and the (turbulent) viscosity.
   (c) Apply boundary conditions on the fine grid velocities u_f^n by interpolating u_c^n to the bounding box.
   (d) $u_c^* = u_c^n + \triangle t(\frac{3}{2}A(u_c^n) - \frac{1}{2}A(u_c^{n-1}))$.
   (e) Calculate the turbulent viscosity ν_t on the fine grid.
   (f) $u_f^* = u_f^n + \triangle t(\frac{3}{2}A(u_f^n) - \frac{1}{2}A(u_f^{n-1}))$.
   (g) Interpolate u_f^* to the coarse grid, ie. $u_c^* = \overline{u}_f^*$ in the overlapping region.
   (h) Determine boundary conditions for u_c^*.
   (i) Solve $-Du_c^* = -\triangle tDGp_c^{n+1}$.
   (j) $u_c^{n+1} = u_c^* - \triangle tGp_c^{n+1}$.
   (k) Determine boundary conditions on the fine grid for u_f^* by interpolating u_c^{n+1} on the bounding box.
   (l) Solve $-Du_f^* = -\triangle tDGp_f^{n+1}$.
   (m) $u_f^{n+1} = u_f^* - \triangle tGp_f^{n+1}$.

Appendix B: Grid-nesting algorithm (2)

1. Initialize u_c^0 and u_f^0.
2. For $n = 1$, nstep do
   (a) Calculate the subgrid stress $\overline{u_i u_j} - \overline{u_i}\ \overline{u_j}$, using the subgrid model in non-nested region and the fine grid solution in the nested region.
   (b) Apply boundary conditions on the coarse grid for the velocities and subgrid stress.
   (c) Apply boundary conditions on the fine grid velocities u_f^n by interpolating u_c^n to the bounding box.
   (d) $u_c^* = u_c^n + \triangle t(\frac{3}{2}A(u_c^n) - \frac{1}{2}A(u_c^{n-1}))$.
   (e) Calculate the turbulent viscosity ν_t on the fine grid.
   (f) $u_f^* = u_f^n + \triangle t(\frac{3}{2}A(u_f^n) - \frac{1}{2}A(u_f^{n-1}))$.
   (g) Solve $-Du_c^* = -\triangle tDGp_c^{n+1}$.
   (h) $u_c^{n+1} = u_c^* - \triangle tGp_c^{n+1}$.
   (i) Determine boundary conditions on the fine grid for u_f^* by interpolating u_c^{n+1} on the bounding box.
   (j) Solve $-Du_f^* = -\triangle tDGp_f^{n+1}$.
   (k) $u_f^{n+1} = u_f^* - \triangle tGp_f^{n+1}$.

References

1. P. J. Mason, Large-eddy simulation: A critical review of the technique. *Q. J. Roy. Met. Soc.* 120 (1994) 1–26.
2. J. P. Boris, F. F. Grinstein, E. S. Oran and R. L. Kolbe, New insights into large eddy simulation. *Fluid Dyn. Res.* 10 (1992) 199–228.
3. M. Germano, U. Piomelli, P. Moin and W. H. Cabot, A dynamic subgrid-scale eddy viscosity model. *Phys. Fluids* 7 (1991) 1760–1765.

4. P. J. Mason and D. J. Thomson, Stochastic backscatter in large-eddy simulations of boundary layers. *J. Fluid Mech.* 242 (1992) 51–78.
5. F. T. M. Nieuwstadt, P. J. Mason, C.-H. Moeng and U. Schumann, Large eddy simulation of the convective boundary layer: A comparison of four computer codes. *Turbulent Shear Flow 8*. Berlin: Springer-Verlag 1992, pp. 343–367.
6. P. Sullivan, C-H. Moeng and J. C. McWilliams, A grid nesting method for large eddy simulation of planetary boundary-layer flows. *Boundary-Layer Meteorology* 80 (1996) 167–202.
7. C.W. Gear, *Numerical Initial Value Problems in Ordinary Differential Equations*. New Jersey: Pretence Hall, 1971, 253pp.
8. J. J. I. M. van Kan, A second-order accurate pressure-correction method for viscous incompressible flow. *SIAM J. Sci. Stat. Comp.* 7 (1986) 870–891.
9. P. N. Swarztrauber, The methods of cyclic reduction Fourier Analysis and the FACR Algorithm for the discrete solution of Poisson's equation on a rectangle. *SIAM Rev.* 19 (1977) 490–501.
10. R. Sweet, Direct methods for the solution of Poisson's equation on a staggered grid. *J. Comp. Phys.* 12 (1973) 422–428.
11. M. C. Thompson and J. H. Ferziger, An adaptive multigrid technique for the incompressible Navier-Stokes equations. *J. Comp. Phys.* 82 (1989) 94–121.
12. M. Lesieur, C. Staquet, P. Le Roy and P. Comte, The mixing layer and its coherence examined from the point of view of two-dimensional turbulence. *J. Fluid Mech.* 192 (1988) 511–534.